Monatshefte für Chemie - Chemical Monthly (2019) 150:2037–2044
https://doi.org/10.1007/s00706-019-02521-4

ORIGINAL PAPER

meso-Substituted BODIPYs as supramolecular building blocks of ordered Langmuir–Blodgett films: structural and morphological characterization

Pamela Cruz del Valle[1] · Montserrat Miranda-Olvera[1] · Violeta Álvarez-Venicio[1] · Martín Caldera-Villalobos[1] · Rafael Arcos-Ramos[1] · Elba Xochitiotzi-Flores[2] · Norberto Farfán[2] · Margarita Rivera[3] · María del Pilar Carreón-Castro[1]

Received: 21 August 2019 / Accepted: 11 November 2019 / Published online: 21 November 2019

Abstract

Two crystalline *meso*-substituted BODIPYs were investigated as supramolecular building blocks of Langmuir–Blodgett (LB) thin films. These sorts of thin films are formed by the transfer of a Langmuir monolayer film of organized amphiphilic molecules onto a solid substrate. In the present contribution, we exploited the capacity of the featured BODIPYs to produce ordered supramolecular self-assemblies through hydrogen-bonding and π-stacking to pre-organize and to control their assembly as LB thin films. Electronic absorption and fluorescence emission of the *meso*-substituted BODIPYs in solution, LB films, and in solid state were studied. The morphology and structure of the LB films were examined by scanning electron microscopy and atomic force microscopy. The structural differences between both BODIPYs have no marked influence on the absorption and fluorescence emission properties in solution. In contrast, absorption properties in solid state (solid samples and LB thin films) depend on the structural nature of the dyes with the appearance of red-shifted bands, which could be an indicator of the presence of aggregates. The supramolecular information contained in the BODIPYs was reflected on the surface characteristics of the featured LB thin films. Both produced homogeneous and uniform films with the presence of some microcrystals, as the number of transferred monolayers increased. These results broaden the capacity of the Langmuir–Blodgett technique to produce ordered and self-assembled thin films of functional small organic molecules (such as BODIPYs) as components of different optoelectronic devices.

Graphic abstract

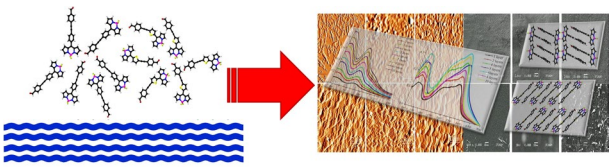

Keywords BODIPYs · Photophysical properties · Self-assembly · Organic semiconductors · Langmuir–Blodgett thin films

Electronic supplementary material The online version of this article (https://doi.org/10.1007/s00706-019-02521-4) contains supplementary material, which is available to authorized users.

✉ Rafael Arcos-Ramos
rafael.arcos@nucleares.unam.mx

✉ María del Pilar Carreón-Castro
pilar@nucleares.unam.mx

[1] Instituto de Ciencias Nucleares, Universidad Nacional Autónoma de México, 04510 Mexico City, Mexico

[2] Departamento de Química Orgánica, Facultad de Química, Universidad Nacional Autónoma de México, 04510 Mexico City, Mexico

[3] Departamento de Materia Condensada, Instituto de Física, Universidad Nacional Autónoma de México, Ciudad Universitaria, 04510 Mexico City, Mexico

Introduction

Nowadays, organic semiconductors represent an efficient alternative to develop charge transport materials as well as light harvesting units for energy conversion processes involved in organic photovoltaics. Particularly, organic semiconductors based on organic π-conjugated small molecules are promising candidates for photovoltaic applications due to their intense and broad absorption profiles, high charge-carrier mobility, and tunable HOMO/LUMO energy levels by chemical functionalization [1–3]. In this sense, thin films with controlled structure and desired properties are required to assure the electronic properties of the organic semiconductor as component of electronics, photovoltaics, or sensors [4–6].

To control the structure and properties displayed by the organic semiconductors, based on organic π-conjugated small molecules, it requires a deep understanding of the supramolecular organization on different condensed matter phases. Therefore, it is necessary to modulate their design, and thus to develop an efficient application as thin solid films [7]. In this sense, translation of the supramolecular information of discrete entities to a regular and ordered molecular packing in thin films requires to take into account some parameters such as chemical structure, physical properties, and capability to self-assembly in solid state. For instance, some Langmuir–Blodgett films of organic semiconductors displayed superior performance characteristics compared with OLEDs constructed by other deposition techniques [8–10].

Amongst the different families of organic compounds, boron-dipyrromethenes (also called BODIPYs) are promising building blocks to construct thin films. These compounds display attractive photophysical properties such as narrow and intense absorption profiles, high fluorescence response, and high photostability as well as chemical and thermal stability. In addition, these properties can be modulated through chemical functionalization of the BODIPY core, *meso*-position as well as over the boron atom depending on the application to achieve [11–16]. A strategy to avoid concentration quenching processes is based on the increasing rigidity of the BODIPY system by the addition of aryl substituents at the *meso* position; this structural modification assures the formation of supramolecular ordered aggregates emissive in the solid state [17].

Therefore, there is a great interest incorporate organic semiconductors, capable to produce molecular crystals into thin films. By exploiting their supramolecular information, it is possible to develop ordered supramolecular structures through the layer-by-layer self-assembly maintaining the photophysical properties of the discrete entities, such as BODIPYs [18–22]. In this sense, we recently reported the synthesis of two novel *meso*-substituted BODIPYs and their assembly in molecular crystals (Fig. 1). These BODIPYs were constructed with a formyl group useful for covalent anchoring to surfaces as well as to develop molecular antennae. After a minutely analysis of the structural and electronic properties by an experimental theoretical approach, we found that π-stacked units of BODIPY play a key role in the self-assembly of a periodic net of overlapping electron density. This intermolecular delocalization of electron density between 2D π-stacked layers could be an indicative of a plausible semiconductor character [23].

Taking into account the mentioned above, herein, we decided to exploit the supramolecular information of BODIPYs **1** (*meso*-[4-[(4-formylphenyl)ethynyl]-phenyl]-4,4-difluoro-4-bora-3a,4a-diaza-*s*-indacene) and **2** (*meso*-[5-[(4-formylphenyl)ethynyl]thiophen-2-yl]-4,4-difluoro-4-bora-3a,4a-diaza-*s*-indacene) to control the

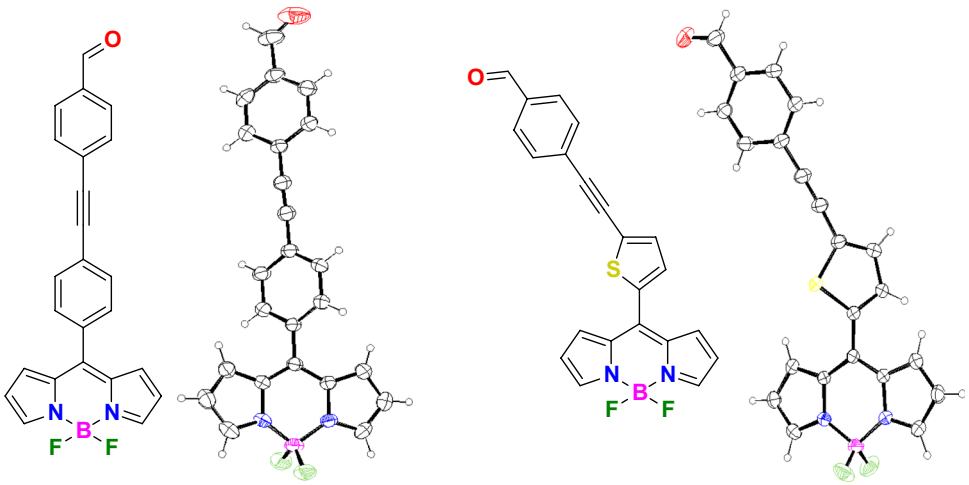

Fig. 1 Chemical structures of *meso*-substituted BODIPYs **1** and **2**

assembly layer by layer of their Langmuir–Blodgett thin films as well as to evaluate the electronic and optical properties. A detailed analysis of the featured BODIPYs in solution and as thin films was carried out by absorbance/fluorescence spectroscopy, atomic force microscopy, and scanning-electron microscopy.

Results and discussion

Photophysical properties of BODIPYs 1, 2 in solution

BODIPYs **1**, **2** were studied through UV–Vis and fluorescence spectroscopy in solution, as illustrated in Figs. 2, 3, the results are summarized in Table 1. An intense absorption band between 501 and 509 and 514–521 nm (for **1** and **2**, respectively) was observed for both due to a π–π* transition of the BODIPY core. Additional absorption bands arise from the donor-π bridge-acceptor π-subsystems (*meso*-substituents). In addition, a batochromically shifted peak was observed in the fluorescence spectra of BODIPYs **1**, **2**. The lower quantum yields can be attributed to the fluorescence quenching caused by the rotation of the alkyne bridges that favored different modes of π-stacking of the BODIPY cores. As we previously reported, these compound exhibit extensive intermolecular π-contacts in the solid state, this particular self-assembly appears to be insensitive in solution to the solvent polarity. The highest Stokes shifts were observed for

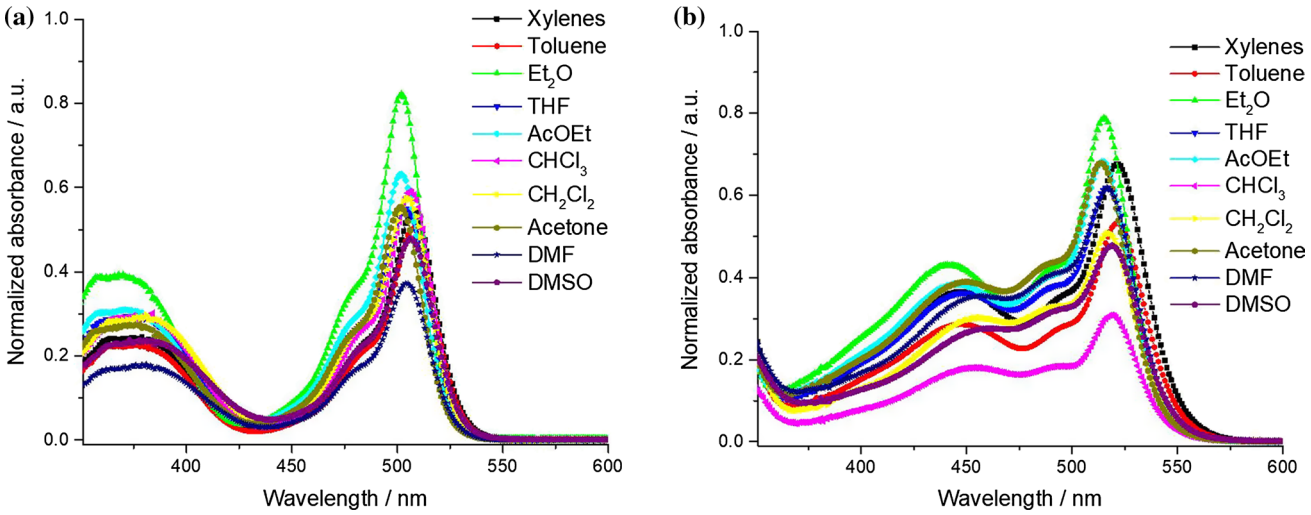

Fig. 2 Absorption profiles of BODIPYs **1**, **2** (concentration 3×10^{-6} mol dm^3)

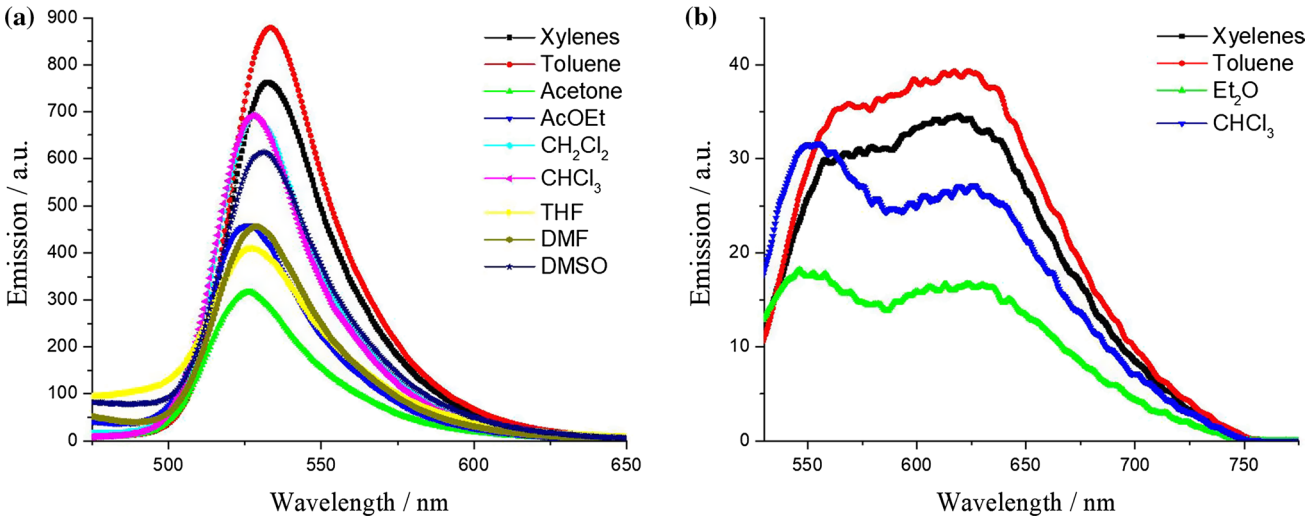

Fig. 3 Fluorescence emission profiles of BODIPYs **1**, **2** (concentration 3×10^{-6} mol dm^3, excitation wavelength $\lambda = 390$ and 510 nm, respectively)

Table 1 Selected photophysical properties of BODIPYs **1**, **2** in solution

BODIPY	Solvent	Absorption λ_{max}/nm	Emission λ_{max}/nm	ε/mol^{-1} dm^3 cm^{-1}	$\Delta\lambda$/nm	ϕ_f
1	Xylenes	507	532	53675.19	25	0.2176
	Toluene	508	534	47603.43	26	0.1297
	Et_2O	502	527	76575.55	25	0.075
	THF	504	524	98630.54	20	0.0869
	AcOEt	502	526	56834.89	24	0.0815
	$CHCl_3$	506	525	51070.18	19	0.1098
	CH_2Cl_2	505	528	48148.20	23	0.1335
	Acetone	501	526	54635.98	25	0.0722
	DMF	504	528	37242.80	24	0.1458
	DMSO	506	530	47444.95	24	0.2031
2	Xylenes	521	625	67162.35	104	0.0089
	Toluene	521	624	51485.44	103	0.00512
	Et_2O	515	630	75367.85	115	0.00391
	THF	517	–	33330.33	–	–
	AcOEt	515	–	68489.71	–	–
	$CHCl_3$	519	626	27934.87	110	0.00748
	CH_2Cl_2	517	–	40082.22	–	–
	Acetone	514	–	6681.40	–	–
	DMF	517	–	61842.86	–	–
	DMSO	519	–	48488.83	–	–

BODIPY **2** (103–115 nm), while BODIPY **1** displayed much lower Stokes shifts (ca. 25 nm).

Langmuir–Blodgett thin-film characterization

Controlled self-assembly is needed to construct complex nanostructures with collective and predetermined properties. Particularly, for device fabrication, ordered patterns are required for practical usage. In this sense, the development of bottom–up methods is desirable due to their accessibility, simplicity, and compatibility with larger scale integration processes. Therefore, the next step was to deposit films of BODIPYs **1**, **2** onto glass substrates to explore their spectral properties and to characterize their morphology. Langmuir monolayers of BODIPYs **1**, **2** were obtained from chloroform solutions at the air–water interface.

Langmuir films were characterized by measuring isotherms surface pressure vs. molecular area (δ vs. A) at 22 °C (Fig. 4a). BODIPYs **1**, **2** exhibited gas phases between 0 and 3 mN m, while the liquid phases were observed at 3–15 mN m (**1**) and 3–13 mN m (**2**). Solid phase for BODIPY **1** was observed between 15 and 66 mN m (molecular area of 15.87 Å^2), whereas for BODIPY **2** was found between 13 and 66 mN M (molecular area of 21.7 Å^2). The large molecular area displayed by BODIPY **2** is due to its molecular structure (non-planar). The lack of axial symmetry within the thiophene derivative avoids a perpendicular approximation to the air–water interface, so it occupies a larger space. The collapse occurred up to 66 mN m, for both. Finally, hysteresis loops (Fig. 4b) show a good reversibility under successive compression–expansion cycles.

The incorporation of the films onto glass substrates was corroborated by Scanning Electron Microscopy (SEM) and Atomic Force Microscopy (AFM). SEM images for 1, 5, and 10 transfers of BODIPYs **1**, **2** are depicted in Fig. 5. For one layer, we observed a homogeneous and compact film covering the complete substrate surface for **2**, in contrast with BODIPY **1**, where there are some areas that are not completely covered (Fig. 5a, d). In the case of 5 transfers (Fig. 5b, e), the homogeneity and uniformity of the films were maintained, with the appearance of spherical aggregates up to 10 µm in diameter scattered along the surface (this could be an indicative of nucleation of nanocrystals). Finally, for 10 transfers (Fig. 5c, f), we observed the appearance of the same aggregates with smaller size giving the film a rougher aspect in comparison with the five-layer films.

In addition, AFM studies were also used to characterize the morphology of the featured films. The incorporation of the films was corroborated by analyzing the decreasing of the substrate surface roughness (Ra) in comparison with the clean substrate. AFM measurements of BODIPYs thin films obtained by the Langmuir–Blodgett technique are presented in Fig. 6. As expected, morphology of the monolayer films depends on the nature of the surface substrate roughness, and one transfer films exhibit elongated aggregates regularly dispersed on the surface with Ra 7.03

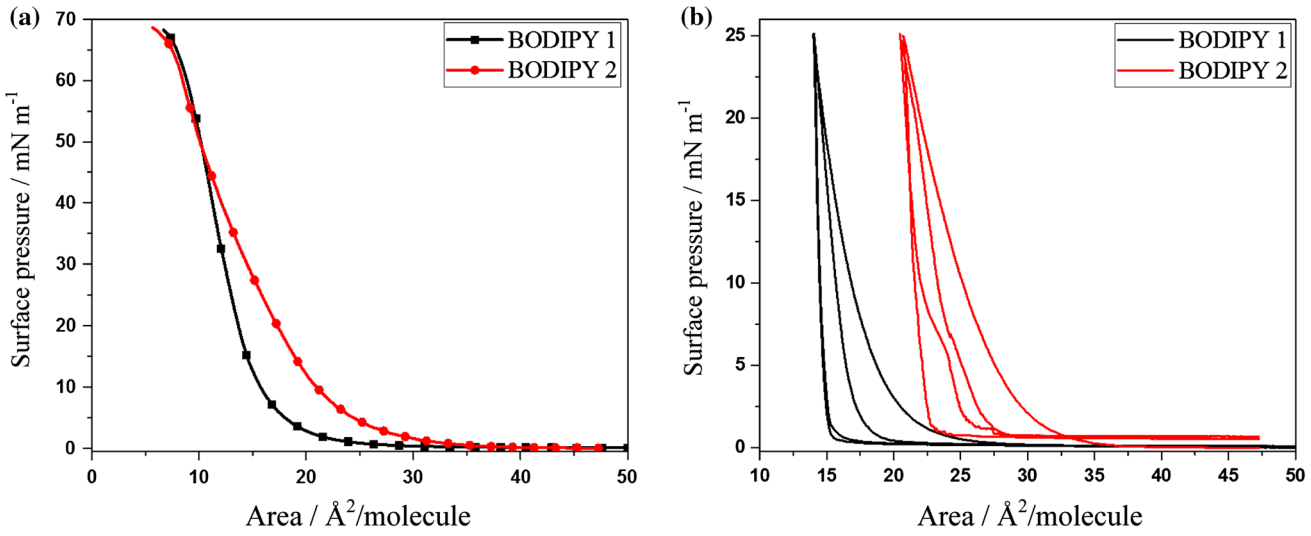

Fig. 4 **a** Surface-pressure-molecular area isotherms (compression rate 10 mm min), and **b** successive compression–expansion cycles (hysteresis) for BODIPYs **1**, **2**

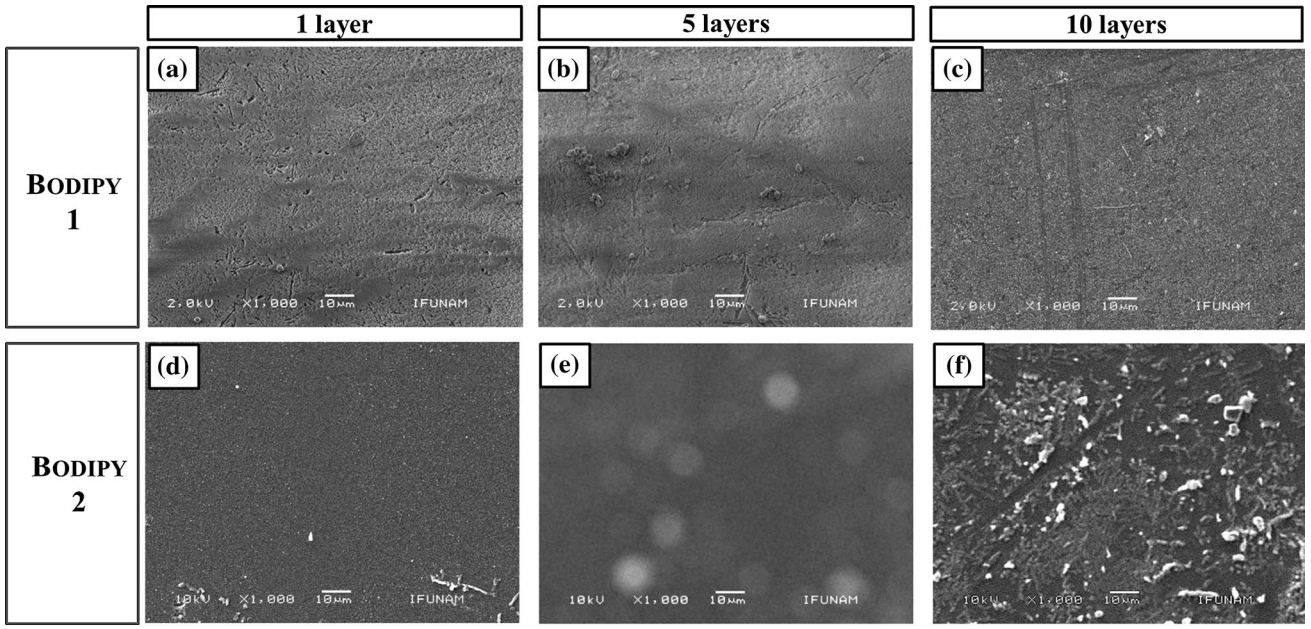

Fig. 5 SEM images of the BODIPYs Langmuir–Blodgett thin films for 1 transfer (**a**, **d**), 5 transfers (**b**, **e**), and 10 transfers (**c**, **f**) for **1** and **2**, respectively (at 1000× magnification)

and 26.5 nm for BODIPYs **1** (maximum height 30 nm) and **2** (maximum height 85 nm), respectively. In addition, film formation arrangements indicated a homogeneous distribution of the BODIPYs during deposition of each successive layer; at 5 transfers, we observed granular uniform patterns on the surface (aggregates with 0.02 μm diameter scattered along the substrate) differing only by their respective roughness of 5.79 (for **1**) and 43.5 nm (for **2**). At 10 transfers, we observed densely packed similar granular patterns, and this closer distribution is reflected on the Ra different values in comparison with the 5 layers films [14.1 nm/70 nm (**1**), and 23.8 nm/160 nm (**2**)]; in the case of BODIPY **2**, the identical height values (5 and 10 layers) suggest that the addition of more layers on the substrate surface does not increase the amount of the deposited compound, only modifies the topography of the film giving it a smoother appearance, which can be an indication that nanocrystals are starting to form. Furthermore, aggregates' orientation in BODIPY **2** (for 5 and 10 transfers) showed a preferential alignment on a particular direction, in contrast with BODIPY **1**, where the

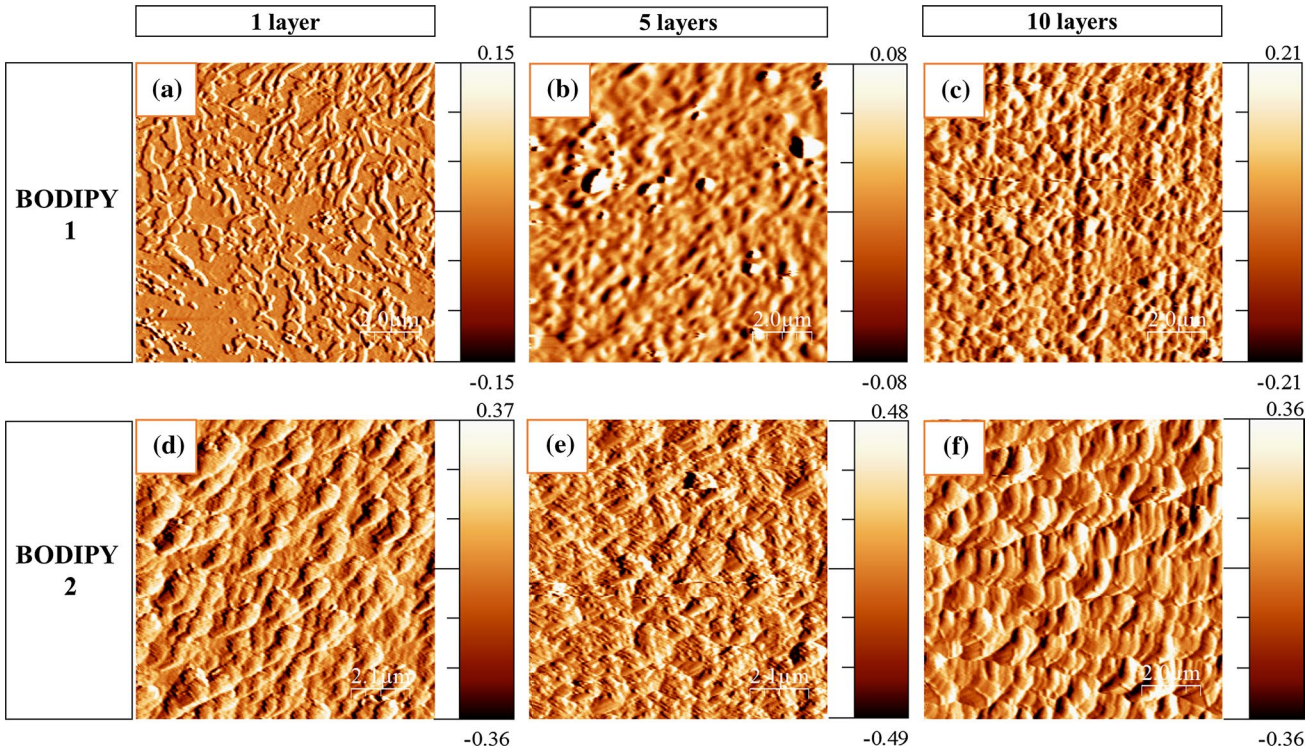

Fig. 6 AFM Images of the BODIPYs Langmuir–Blodgett thin films for 1 transfer (**a**, **d**), 5 transfers (**b**, **e**), and 10 transfers (**c**, **f**) for **1** and **2**, respectively (scale 20 × 20 µm)

misalignment of the aggregates can be responsible for the non-linearity of their UV–Vis plots.

As expected, BODIPYs **1**, **2** are capable to produce ordered supramolecular arrangements on their LB thin films; however, BODIPY **1** displayed higher ordered supramolecular structures as the number of deposited layers increase, this behavior can be explained by the capacity of compound **1** to establish intermolecular contacts between parallel subunits with π-electron density, which in the case of BODIPY **2** is not present due to the lack of axial symmetry within the thiophene fragment (reflected in alternation in the layered structure of their molecular crystal and in a larger molecular area on their LB thin films.

Langmuir–Blodgett thin-film absorption studies

Absorption spectra of BODIPYs **1**, **2** (freshly recrystallized solid samples) and in chloroform solutions are presented in Fig. 7. BODIPY **1** features three main absorption bands at about 375, 485, and 605 nm. All are rather broad and span the entire region between 350 and 750 nm, being the most intense the 375 nm band (which correspond with π–π* transitions involving the donor-bridge-acceptor π-subsystem). In addition, a similar behavior was found in BODIPY **2**, with the difference that two additional bands appeared at 675 and 740 nm, probably due to the different modes of π-stacking between the BODIPY cores. Nonetheless, focusing on the shape of the main bands, we can identify a more complex structure, composed of at least three different components, where only one band coincided with the absolute maximum found in chloroform solutions; these results suggest interesting effects of controlled self-assembly on the optical properties of the BODIPYs.

As we previously described, BODIPY **1** and **2** Langmuir monolayers were transferred onto solid glass substrates using the Langmuir–Blodgett technique (vertical lifting method), with transfer ratios of ca. 1 ± 0.2 on Z-type deposition. Absorption spectra of BODIPYs **1**, **2** are depicted in Fig. 8; both dyes displayed a bathochromic shift (22 and 25 nm for **1** and **2**, respectively) in comparison with chloroform solutions. The appearance of red-shifted bands (LB films and solid samples) could be an indicative of the presence of *J*-aggregates (due to the capacity to self-assembly of the dyes by hydrogen-bonding and π-stacking interactions).

Conclusion

Two *meso*-substituted BODIPYs were used as supramolecular building blocks to construct ordered and self-assembled Langmuir–Blodgett thin films; BODIPYs **1**, **2** were capable to produce Langmuir monolayers at the air–water interface,

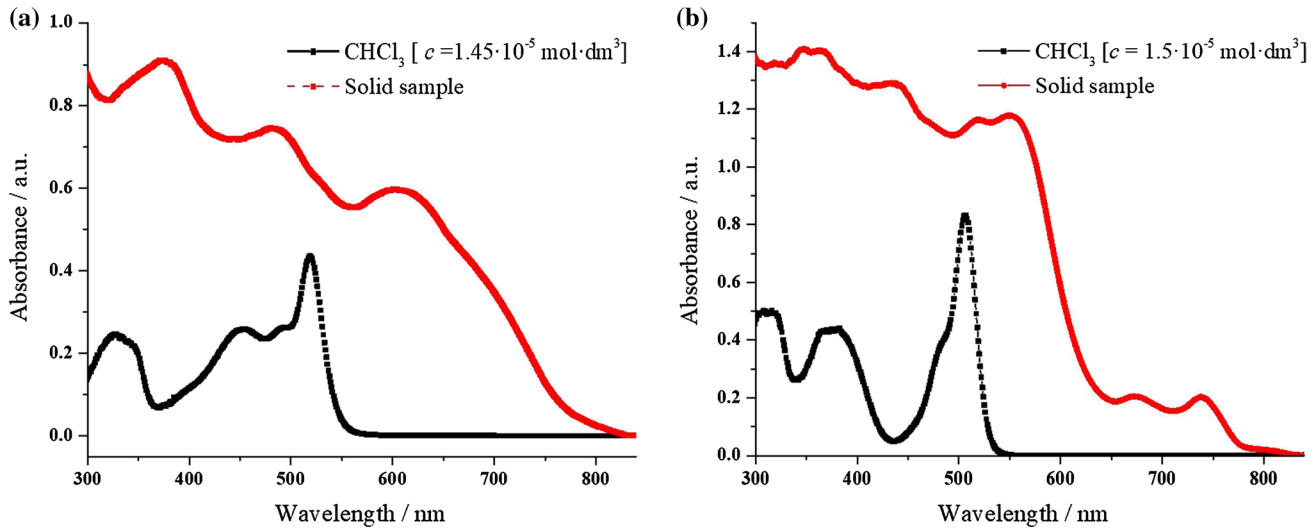

Fig. 7 Absorption spectra of solid samples and chloroform solutions of BODIPYs (**a**) **1**, and (**b**) **2**

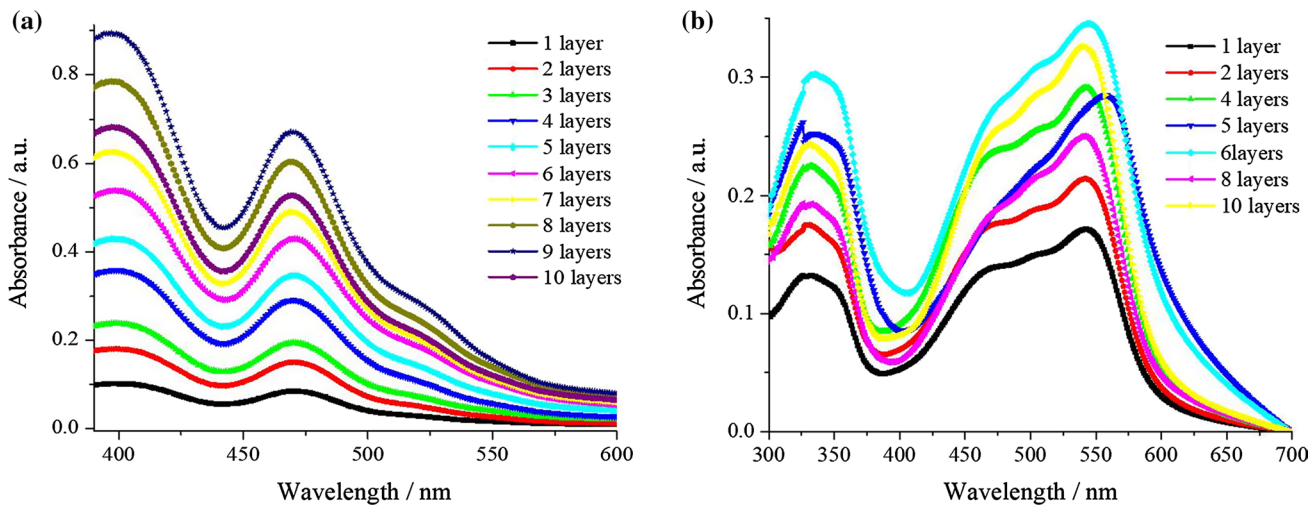

Fig. 8 Absorption spectra of Langmuir–Blodgett films of **a** BODIPY **1**, and **b** BODIPY **2**

and the featured films were characterized by surface pressure vs. molecular area isotherms exhibiting excellent stability upon successive compression–expansion cycles (hysteresis). Langmuir monolayers (up to 10) were transferred onto glass substrates to form Langmuir–Blodgett thin films, which were characterized by electron microscopy (SEM and AFM) as well as by UV/Vis spectroscopy. The featured dyes as thin films displayed a bathochromic shift (22 and 25 nm for **1** and **2**, respectively) in comparison with chloroform solutions. The appearance of red-shifted bands (thin films and solid-state samples) could be an indicative of the presence of *J*-aggregates (due to the capacity to self-assembly of the dyes by hydrogen-bonding and π-stacking interactions). These results broaden the capacity of the Langmuir–Blodgett technique to produce ordered and self-assembled thin films of functional small organic molecules (such as BODIPYs) as components of different optoelectronic devices.

Experimental

NMR experiments were recorded in $CDCl_3$ solution in a JEOL Eclipse 400 spectrometer; chemical shifts are reported in ppm with respect to TMS using residual solvent signal (fixed at $\delta = 7.26$ ppm for ^1H and $\delta = 77.160$ ppm for ^{13}C), coupling constants (*J*) are in Hz. Boron NMR spectra were referenced to external $BF_3{\cdot}Et_2O$ in $CDCl_3$ (fixed at $\delta = 0$ ppm). Fluorine NMR spectra were referenced to $CFCl_3$

(fixed at $\delta = 0$ ppm). Absorption studies were performed on a UV/VIS Lambda 35 Perkin Elmer spectrophotometer. Fluorescence emission studies were acquired on a LS55 Perkin Elmer fluorescence spectrometer. Scanning electron microscopy images were acquired on a JEOL SEM5600LV instrument at 15 kV and different magnifications. Atomic force microscopy images were obtained with a JEOL JSPM4210 instrument in tapping mode.

Synthesis

BODIPYs **1**, **2** were synthesized in good yields using our previously reported methodology; both compounds were recrystallized from acetone before use [23].

Langmuir Monolayers

Spreading solutions of 0.001 mg cm^3 were prepared in $CHCl_3$ for BODIPYs **1**, **2**; ASTM type 1 ultrapure water was employed for the subphase (Milli-Q system, 18.2 MΩ cm and simplicity 185, Millipore). Preparation of the corresponding monolayers was carried out on a KSV 5000 alternate multilayer LB system (KSV Finland). Different amounts of BODIPY solutions (0.2–0.24 cm^3) were slowly spread over the water surface; the system was maintained undisturbed for 15 min to achieve a complete chloroform evaporation. Afterwards, the monolayer was symmetrically compressed (barrier speed 10 mm min), and the surface-pressure isotherms were acquired at 22 °C according to the Wilhelmy method. Finally, monolayers' stability was determined through compression–expansion cycles (hysteresis loops) below the collapse pressure.

Langmuir–Blodgett thin films

Langmuir monolayers of BODIPYs **1**, **2** were transferred onto solid glass substrates ($35 \times 13 \times 1$ mm^3) using the vertical lifting method (transfer ratio of 1 ± 0.2) at 22 °C. Glass substrates were previously treated with a sulfochromic solution, ultrapure water, ethanol, and chloroform to remove impurities. Z-type multilayer structures ($n = 1$–10 layers) were prepared by vertical deposition method (extraction only) at pressures between 0 and 70 mN m and dipping speed of 10 mm min.

Acknowledgements MDP Carreón-Castro acknowledges to DGAPA-UNAM (PAPIIT IN-206018). M.M.O. and P.C.V. acknowledge to CONACYT for the granted PhD scholarships (Grants numbers 335895 and 288878, respectively). V. Alvarez-Venicio acknowledges to CONACYT for the cathedra 411-2016. M. Caldera-Villalobos thanks to DGAPA-UNAM for the granted postdoctoral fellowship. The authors would like to express their gratitude to Manuel Aguilar Franco, Jacqueline R. D. Cañetas Ortega, and Diego Quiterio Vargas (IF-UNAM) for technical assistance.

References

1. Inganäs O (2018) Adv Mater 30:1800388
2. Zhang X, Dong H, Hu W (2018) Adv Mater 30:1801048
3. Kim FS, Ren G, Jenekhe SA (2011) Chem Mater 23:682
4. Riera-Galindo S, Tamayo A, Mas-Torrent M (2018) ACS Omega 3:2329
5. Miao Q (2014) Adv Mater 26:5541
6. Virkar AA, Mannsfeld S, Bao Z, Stingelin N (2019) Adv Mater 22:3857
7. Yang J, Yan D, Jones TS (2015) Chem Rev 115:5570
8. Fernández-Hernández JM, De Cola L, Bolink HJ, Clemente-León M, Coronado E, Forment-Aliaga A, López-Muñiz A, Repetto D (2014) Langmuir 30:14021
9. Yang Y, Yang X, Lo S, Xu J, Jiang Y (2014) Nanoscale Res Lett 9:537
10. Dhrubojyoti R, Mani DN, Shakti N, Gupta PS (2014) RSC Adv 80:42514
11. Lakshmi V, Rajeswara Rao M, Ravinkath M (2015) Org Biomol Chem 13:2501
12. Mack J, Yang Y, Shen Z (2014) Chem Soc Rev 43:4778
13. Luo L, Wu D, Li W, Zhang S, Ma Y, Yan S, You J (2014) Org Lett 16:6080
14. Xiao S, Cao Q, Dan F (2012) Curr Org Chem 16:2970
15. Suzuki S, Kozaki M, Nozaki K, Okada K (2011) J Photochem Photobiol, C 12:269
16. Ulrich G, Ziessel R, Harriman A (2008) Angew Chem Int Ed 47:1184
17. Hong Y, Lam JWY, Tang BZ (2011) Chem Soc Rev 40:5361
18. Ho D, Ozdemir R, Kim H, Earmme T, Usta H, Kim C (2019) ChemPlusChem 84:18
19. Yilmaz M, Erkatal M, Ozdemir M, Sen U, Usta H, Demirel G (2017) ACS Appl Mater Interfaces 9:18199
20. Vithange DA, Manousiadis PP, Sajjad MT, Rajbhandari S, Chun H, Orofino C, Cortizo-Lacalle D, Kanibolotsky AL, Faulkner G, Findlay NJ, O'Brien DC, Skabara PJ, Samuel IDW, Turnbull GA (2016) Appl Phys Lett 109:013302
21. Corona-Sánchez R, Arcos-Ramos R, Maldonado-Domínguez M, Amelines-Sarria O, Jerezano-Domínguez A, García-Ortega H, Rivera M, Carreón-Castro MP, Farfán N (2016) Monatsh Chem 147:1915
22. Mueller T, Gresser R, Leo K, Riede M (2012) Sol Energy Mater Sol Cells 99:176
23. Xochitiotzi-Flores E, Islas-Mejía AA, García-Ortega H, Romero-Avila M, Mendez-Stivalet JM, Carreón-Castro MP, Santillan R, Maldonado-Domínguez M, Arcos-Ramos R, Farfán N (2016) J Organomet Chem 805:148